J. Plasma Physics (2005), *vol.* 71, *part* 5, *pp.* 675–693. © 2005 Cambridge University Press
doi:10.1017/S0022377805003636 Printed in the United Kingdom

On electron Bernstein waves in spherical tori

ABHAY K. RAM[1], JOAN DECKER[1] and YVES PEYSSON[2]

[1]Plasma Science and Fusion Center, Massachusetts Institute of Technology, Cambridge, MA 02139, USA
(abhay@psfc.mit.edu)

[2]Association Euratom – CEA, 13108 St. Paul-lez-Durance, Cadarache, France

(Received 1 September 2005)

Abstract. The high-β operating regime of spherical tori (ST), such as in the National Spherical Torus Experiment (NSTX) and the Mega Amp Spherical Tokamak (MAST), makes them attractive fusion devices. For access to such high-β regimes it is necessary to heat and to drive currents in ST plasmas. In the electron cyclotron range of frequencies, such plasmas are overdense to conventional electron cyclotron waves. However, in this frequency range, electron Bernstein waves (EBWs) offer an attractive alternative as they have no density cutoffs. EBWs can be excited in a ST plasma by mode conversion of the extraordinary or the ordinary mode at the upper hybrid resonance. The applications of EBWs in STs range from plasma start-up and heating of the plasma to modifying and controlling its current profile. The controlling of the current profile could provide better confinement as well as help suppress neoclassical tearing modes. The mode conversion to EBWs has been detailed in a variety of papers. This paper deals with two particular topics that further quantify the role of EBWs in spherical tori. The first topic is on the relevance of relativistic effects in describing the propagation and damping of EBWs. The second topic is on plasma current generation by EBWs.

1. Introduction

In order to achieve high-β plasmas, spherical tori (ST) such as the National Spherical Torus Experiment (NSTX) [1] and Mega Amp Spherical Tokamak (MAST) [2] generally operate at low magnetic fields and high densities such that $\omega_{pe}/\omega_{ce} \gg 1$ over most of the plasma. Here ω_{pe} and ω_{ce} are the angular electron plasma and cyclotron frequencies, respectively. Such an overdense nature of ST plasmas makes them unsuitable for heating and/or current drive by the conventional ordinary O and extraordinary X modes in the electron cyclotron (EC) range of frequencies. For low harmonics of ω_{ce} the X and O modes are cut off near the edge of the plasma. For high harmonics, these modes access the core of the ST plasma, but are essentially undamped when they encounter the EC resonances. However, electron Bernstein waves (EBWs) offer an attractive alternative in the EC frequency range as they have no density cutoffs, and damp strongly on electrons at the fundamental or any harmonic of the Doppler-shifted EC resonance [3]. Since EBWs cannot propagate in vacuum (like the X and O modes) they are excited, indirectly, by mode conversion of an externally launched O mode or X mode [3–6]. Successful

https://doi.org/10.1017/S0022377805003636 Published online by Cambridge University Press

experiments on mode conversion excitation of EBWs and their subsequent interaction with the plasma have been summarized by Laqua [7].

In studying the propagation and damping of the traditional X and O modes in the EC frequency range it has been noted that weakly relativistic effects are important [8–10]. Motivated by these studies we have developed a numerical code R2D2 to determine the relativistic modifications to the propagation and damping of EBWs. R2D2 solves the fully relativistic wave dispersion relation instead of the weakly relativistic approximation used for studying conventional EC waves. Away from the mode conversion region, as the waves propagate into the interior of a toroidal plasma, the perpendicular (to the magnetic field) wavelength $\lambda_\perp$ of EBWs shortens and is comparable with, or less than, the electron Larmor radius ρ_e [3]. Consequently, in contrast to the case of X and O modes, we cannot carry out small $\rho_e/\lambda_\perp$ expansions of the dielectric tensor elements for EBWs. Our initial results from R2D2 indicate that relativistic effects are important for EBWs in a ST plasma away from the mode conversion edge region.

An important role for EBWs in STs would be to generate non-inductive plasma currents [11, 12]. A study of the propagation of EBWs in a toroidal equilibrium using a non-relativistic ray trajectory code shows that the parallel wave number $n_\parallel = ck_\parallel/\omega$ can change from well below 1 to above 1 along the ray path [3]. ($k_\parallel$ is the component of the wave vector parallel to the magnetic field, c is the speed of light, and ω is the wave angular frequency.) The changes in $n_\parallel$ are primarily due to the poloidal magnetic field. Consequently, the accessible phase space for current drive by EBWs is richer than for the X and O modes. For the X and O modes the resonance surfaces, in electron momentum space, for the wave–electron interactions are elliptic while the electron diffusion paths lie along hyperbolas. The resonance surfaces and diffusion paths for EBWs also have the same properties for $n_\parallel < 1$. However, in addition, for EBWs with $n_\parallel > 1$ the resonance surfaces are hyperbolas and the diffusion paths become elliptic. A drift kinetic Fokker–Planck code DKE [13], which includes a quasilinear RF diffusion operator and the effect of trapped electrons, is being used to study EBW current drive. The code is fully relativistic as are the collision operator and the quasilinear diffusion operator. The latter includes the relativistic wave–particle resonance condition. Numerical results obtained using DKE show that in the outer half of a ST plasma, where the trapped electron population is significant, EBWs effectively drive current through the Ohkawa mechanism [14,15]. In the core of the plasma where the fraction of trapped electrons is reduced, EBWs effectively generate current through the Fisch–Boozer scheme [16].

2. Relativistic conductivity tensor

The relativistic formulation of the plasma dielectric tensor in a homogeneous plasma has been previously discussed by Trubnikov [17] and Shkarofsky [18]. For waves in the EC range of frequencies, the ion dynamics can be neglected so that the dielectric tensor only includes the electron contribution. Here we follow the formalism due to Trubnikov [17].

The dielectric tensor is evaluated in a slab geometry with (x, y, z) being the appropriate coordinates. The plasma is assumed to be immersed in a uniform magnetic field $\mathbf{B}_0 = B_0\hat{z}$ pointing in the z-direction. Then the unperturbed distribution function f_0 for the electrons is a function of $p_\perp$ and $p_\parallel$, the components of the momentum perpendicular and parallel to $\mathbf{B}_0$, respectively. We assume an electromagnetic wave

https://doi.org/10.1017/S0022377805003636 Published online by Cambridge University Press

propagating in the plasma with an electric field of the form

$$\mathbf{E} = (E_x, E_y, E_z)e^{i\mathbf{k}\cdot\mathbf{r}-i\omega t}, \tag{1}$$

where $\mathbf{k}$ and ω are the wavevector and angular frequency, respectively. The corresponding wave magnetic field is given by Maxwell's equations. Then, from the linearized Vlasov equation, the perturbed electron distribution function is

$$f_1 = -\frac{1}{\Omega}\exp\left\{\frac{-i}{\Omega}\left(\lambda\phi - \frac{p_\perp k_\perp}{m\gamma}\sin(\phi-\psi)\right)\right\} \times \int_{-\infty}^{\phi} d\phi' \exp\left\{\frac{i}{\Omega}\left(\lambda\phi' - \frac{p_\perp k_\perp}{m\gamma}\sin(\phi'-\psi)\right)\right\}\hat{P}' f_0(p_\perp, p_\parallel), \tag{2}$$

where m is the rest mass of an electron, c is the speed of light,

$$\frac{\hat{P}}{-q} = \frac{1}{\sqrt{2}}(E_l e^{-i\phi} + E_r e^{i\phi})\hat{G} + E_\parallel\left(\frac{k_\perp}{\omega}\cos(\psi-\phi)\hat{H} + \frac{\partial}{\partial p_\parallel}\right), \tag{3}$$

$$\hat{G} = \frac{\partial}{\partial p_\perp} - \frac{k_\parallel}{\omega}\hat{H}, \quad \hat{H} = \frac{p_\parallel}{m\gamma}\frac{\partial}{\partial p_\perp} - \frac{p_\perp}{m\gamma}\frac{\partial}{\partial p_\parallel}, \tag{4}$$

$$\lambda = \omega - \frac{k_\parallel p_\parallel}{m\gamma}, \quad \gamma = \left(1 + \frac{p_\perp^2}{m^2c^2} + \frac{p_\parallel^2}{m^2c^2}\right)^{1/2}, \quad \Omega = \frac{qB_0}{m\gamma}, \tag{5}$$

$$p_x = p_\perp\cos(\phi), \quad k_x = k_\perp\cos(\psi), \quad \sqrt{2}E_{l,r} = E_x \pm iE_y. \tag{6}$$

The plasma conductivity tensor $\overline{\overline{\sigma}}$ is obtained from the current density

$$\mathbf{j} = en_0\int d^3p\frac{\mathbf{p}}{m\gamma}f_1 = \overline{\overline{\sigma}}\cdot\mathbf{E} \tag{7}$$

where e is the electron charge and n_0 is the unperturbed electron density. Here we have assumed that the unperturbed distribution function f_0 leads to no current in the plasma.

From (2) and (7) we note that there are two integrals that need to be evaluated in order to determine $\overline{\overline{\sigma}}$. One integral is essentially the time history integral over ϕ' and the other integral is over the momentum space $\mathbf{p}$. Let us assume that f_0 is a relativistic Maxwellian

$$f_0(p_\perp, p_\parallel) = \frac{1}{4\pi}\frac{1}{T_e}\frac{1}{m^2c}\frac{1}{K_2(mc^2/T_e)}e^{-(\gamma mc^2/T_e)}, \tag{8}$$

where T_e is the electron temperature (in energy units), and K_ν is the modified Bessel function of the second kind of order ν. In this case the two integrals together cannot be carried out analytically. Consequently, there are two complementary approaches for obtaining $\overline{\overline{\sigma}}$ [17]. The first is to perform the momenta integrals analytically and then evaluate the time history ϕ' integral in (2) numerically. The second technique is to perform the ϕ' integral analytically and then evaluate the momenta integrals in (7) numerically. The two forms of $\overline{\overline{\sigma}}$ obtained from these different approaches are given below.

https://doi.org/10.1017/S0022377805003636 Published online by Cambridge University Press

2.1. Analytical evaluation of the momenta integrals

For a relativistic Maxwellian distribution function the analytical evaluation of the momenta integrals leads to

$$\overline{\overline{\sigma}} = \frac{1}{4\pi}\frac{\omega_{\rm pe}^2}{\omega_{\rm ce}}\frac{c^4}{v_{\rm te}^4}\frac{1}{K_2(c^2/v_{\rm te}^2)}\int_0^\infty d\xi\left\{\frac{K_2(R^{1/2})}{R}\overline{\overline{T}}_1 - \frac{K_3(R^{1/2})}{R^{3/2}}\overline{\overline{T}}_2\right\}, \tag{9}$$

where $\omega_{\rm pe}$, $\omega_{\rm ce}$, $v_{\rm te} = \sqrt{T_{\rm e}/m}$ are the rest mass electron plasma frequency, cyclotron frequency, and the thermal velocity, respectively,

$$\overline{\overline{T}}_1 = \begin{pmatrix} \cos\xi & -\sin\xi & 0 \\ \sin\xi & \cos\xi & 0 \\ 0 & 0 & 1 \end{pmatrix} \tag{10}$$

$$\overline{\overline{T}}_2 = \frac{c^2}{\omega_{\rm ce}^2}\begin{pmatrix} k_\perp^2\sin^2\xi & -k_\perp^2\sin\xi\,(1-\cos\xi) & k_\perp k_\parallel\xi\sin\xi \\ k_\perp^2\sin\xi\,(1-\cos\xi) & -k_\perp^2\,(1-\cos\xi)^2 & k_\perp k_\parallel\xi\,(1-\cos\xi) \\ k_\perp k_\parallel\xi\sin\xi & -k_\perp k_\parallel\xi\,(1-\cos\xi) & k_\parallel^2\xi^2 \end{pmatrix} \tag{11}$$

$$R = \left(\frac{c^2}{v_{\rm te}^2} - i\xi\frac{\omega}{\omega_{\rm ce}}\right)^2 + 2\left(\frac{k_\perp c}{\omega_{\rm ce}}\right)^2(1-\cos\xi) + \frac{k_\parallel^2 c^2\xi^2}{\omega_{\rm ce}^2}. \tag{12}$$

We are now left to evaluate the integral in (9) numerically. It is interesting to note that if we make the appropriate approximations corresponding to a non-relativistic Maxwellian as the unperturbed distribution function, the familiar results [19] are readily obtained as the integral in (9) can be carried out analytically.

2.2. Analytical evaluation of the time history integral

If, instead of the momenta integrals, we carry out the time history integral in (2), then

$$\overline{\overline{\sigma}} = -\frac{i}{2}\frac{\omega_{\rm pe}^2}{\omega_{\rm ce}}\left\langle\sum_{n=-\infty}^{\infty}\frac{1}{T_{\rm e}}\left(\frac{1}{n-\overline{\omega}}\right)\frac{p_\perp}{m\gamma}\overline{\overline{\sigma}}_N f_0(p_\perp,p_\parallel)\right\rangle, \tag{13}$$

where

$$\overline{\overline{\sigma}}_N = \begin{pmatrix} \dfrac{n^2}{\zeta^2}p_\perp J_n^2 & -i\dfrac{n}{\zeta}p_\perp J_n J_n' & \dfrac{n}{\zeta}p_\parallel J_n^2 \\ i\dfrac{n}{\zeta}p_\perp J_n J_n' & p_\perp J_n'^2 & ip_\parallel J_n J_n' \\ \dfrac{n}{\zeta}p_\parallel J_n^2 & -ip_\parallel J_n J_n' & \dfrac{p_\parallel^2}{p_\perp}J_n^2 \end{pmatrix}, \tag{14}$$

$$\zeta = \frac{k_\perp p_\perp}{m\omega_{\rm ce}}, \quad \overline{\omega} = \frac{1}{\omega_{\rm ce}}\left(\omega\gamma - k_\parallel\frac{p_\parallel}{m}\right), \quad \omega_{\rm ce} = \frac{eB_0}{m}, \tag{15}$$

$J_n = J_n(\zeta)$ is the ordinary Bessel function of the first kind of order n, and

$$\langle\ldots\rangle = \int_0^\infty dp_\perp\, p_\perp\int_{-\infty}^{\infty}dp_\parallel. \tag{16}$$

https://doi.org/10.1017/S0022377805003636 Published online by Cambridge University Press

3. Relativistic dispersion relation

The use of the perturbed current density (7) in Maxwell's equations leads to the relativistic dispersion tensor

$$\overline{\overline{D}}(\mathbf{k},\omega) = \frac{c^2}{\omega^2}\mathbf{kk} + \left(1 - \frac{c^2k^2}{\omega^2}\right)\overline{\overline{I}} + \frac{4\pi i}{\omega}\overline{\overline{\sigma}}, \tag{17}$$

where $\overline{\overline{I}}$ is the unit tensor and $\mathbf{kk}$ is a dyadic. The dispersion relation for waves in the EC range of frequencies is obtained by setting the determinant $\det(\overline{\overline{D}})$ to zero.

We have developed a code R2D2 that solves $\det[\overline{\overline{D}}(\mathbf{k},\omega)] = 0$ for the dispersion characteristics of EC waves using two separate and distinct numerical routines. One routine uses (9) for $\overline{\overline{\sigma}}$ in (17) while the other routine uses (13). The latter routine uses some of the features discussed in [20]. Since we are not aware of any similar code in existence, the independent routines allow us to benchmark our own code. For a variety of cases we find that the two routines provide numerically identical results leading us to have confidence in our code.

4. Numerical comparison of relativistic and non-relativistic dispersion characteristics

We have used R2D2 to compare the relativistic and non-relativistic dispersion characteristics of EC waves for various parameters. In Fig. 1 we compare the results obtained from the relativistic description with those obtained from the non-relativistic description in the mode conversion region for NSTX model equilibrium [3]. The dispersion characteristics are along the equatorial plane of the model NSTX plasma, where x corresponds the radial distance [3]. Here $x = 44$ cm is the outside edge of the plasma and $x = 0$ cm corresponds to the center of the plasma. We note that there is essentially no difference between the two cases in the low-temperature region where the mode coupling takes place. Thus, the mode conversion formalism developed in [3–6] is not modified by relativistic effects in a ST where the conversion takes place near the edge of the plasma. However, the EBW part of the dispersion relation begins to show some differences away from the mode conversion region. In Fig. 2 we show the dispersion characteristics of EBW as a function of distance into the plasma away from the mode conversion region. The imaginary part of $n_\perp$ in Fig. 2(b) shows the relativistic Doppler broadening of the EBW near the fourth harmonic of the EC frequency. Clearly, the damping of the EBW will occur further away from the cyclotron resonance than would be expected from the non-relativistic dispersion relation. The change in the real part of $n_\perp$ in Fig. 2(a) is related to the magnetic field profile in the case of high-β scenarios [3]. The magnetic field has a well-like shape. The total field initially decreases along the equatorial plane as a function of distance into the plasma starting from the outside edge. At about half the minor radius the total magnetic field begins to increase.

In order to illustrate the effect of various parameters on the differences between the relativistic and non-relativistic EBW dispersion characteristics we consider several cases. The dispersion relation can, in general, be expressed as a function of $n_\perp$, $n_\parallel$, ω, T_e, ω_{pe}/ω_{ce}, and ω/ω_{ce}. We solve the real and imaginary parts of $n_\perp$ as a function of one of the other parameters. The rest are kept fixed at some value.

In Fig. 3 we show the changes in $n_\perp$ as a function of ω/ω_{ce} for EBWs in a uniform plasma with $T_e = 3$ keV, $\omega_{pe}/\omega_{ce} = 6$, and $n_\parallel = 0.2$. As the EBW approaches

https://doi.org/10.1017/S0022377805003636 Published online by Cambridge University Press

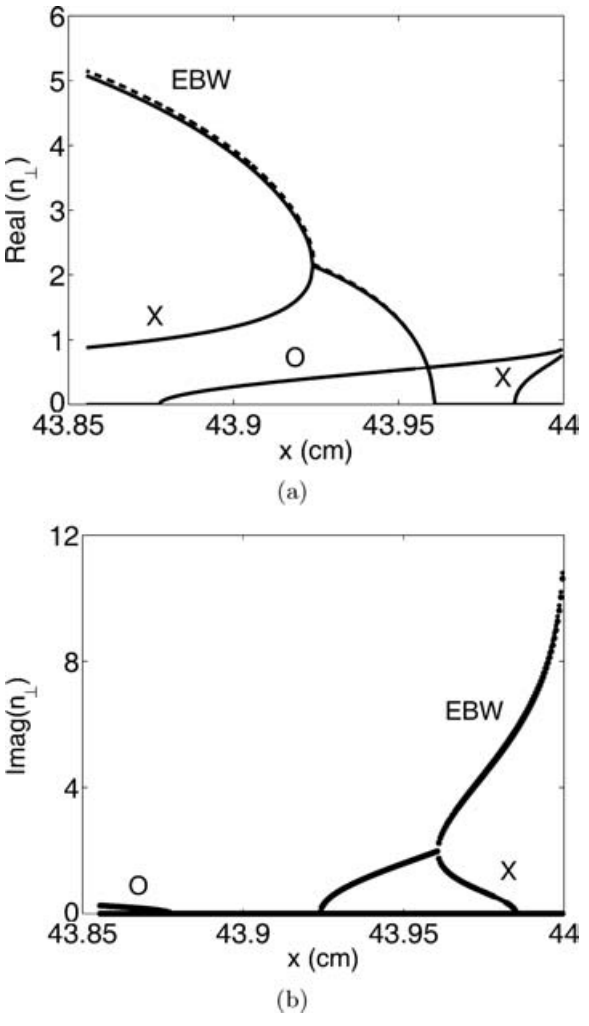


Figure 1. (a) Real and (b) imaginary part of $n_\perp = ck_\perp/\omega$ versus distance along the equatorial plane for NSTX-type parameters [3]. The comparison is between the relativistic (solid) and the non-relativistic (dashed) characteristics of EC waves in the mode conversion region. $x =$ 44 cm is the outside edge of the plasma and $x = 0$ cm is the center of the plasma. The results are for $n_\parallel = ck_\parallel/\omega = 0.1$ and a wave frequency of 15 GHz.

the second cyclotron harmonic from the high field side, relativistic effects broaden the Doppler-shifted cyclotron resonance. However, as the EBW approaches the fundamental EC resonance from the low field side, relativistic effects narrow the Doppler-shifted cyclotron resonance.

In Fig. 4 we show the changes in $n_\perp$ as a function of $n_\parallel$ for EBWs in a uniform plasma with $T_e = 3$ keV, $\omega_{pe}/\omega_{ce} = 6$, and $\omega/\omega_{ce} = 1.8$. From ray tracing, it has been shown that, for EBWs, $n_\parallel$ can range from being below 1, as for the X and O modes, to above 1 as the EBWs propagate in a toroidal equilibrium [3]. The differences between the relativistic and non-relativistic values of real and imaginary parts of $n_\perp$ show that a relativistic formalism for the ray equations may be necessary to determine the path and the damping of EBWs in a toroidal equilibrium.

https://doi.org/10.1017/S0022377805003636 Published online by Cambridge University Press

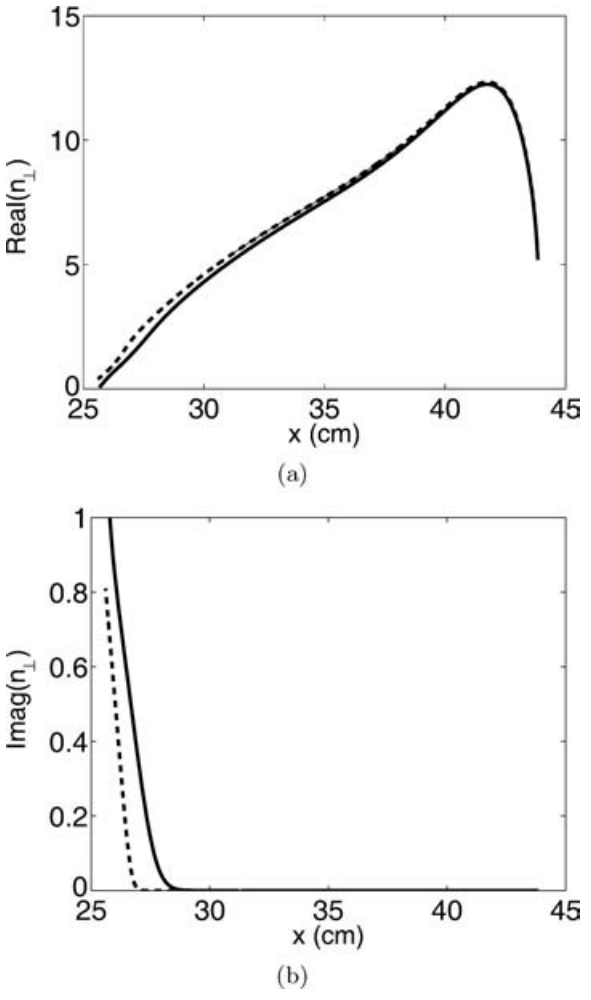


Figure 2. (a) Real and (b) imaginary part of $n_\perp$ versus distance for EBWs. The comparison is between the relativistic (solid) and the non-relativistic (dashed) characteristics of EBWs. The equilibrium parameters are the same as for Fig. 1.

The cumulative effect of the differences in the dispersion properties as $n_\parallel$ changes along an EBW ray path in a toroidal geometry could lead to important changes in the location of wave damping on electrons.

Figures 5(a) and 5(b) show the differences between the relativistic and non-relativistic dispersion characteristics of EBWs as a function of temperature. As the figures illustrate, differences start to occur at electron temperatures below 1 keV. From different numerical results we find that the differences persist but decrease as $n_\parallel$ increases. These results signify the relevance of including relativistic effects in the propagation and damping of EBWs. A relativistic ray-tracing code based on R2D2 is being developed to further elucidate the differences along ray paths in toroidal plasma equilibria.

https://doi.org/10.1017/S0022377805003636 Published online by Cambridge University Press

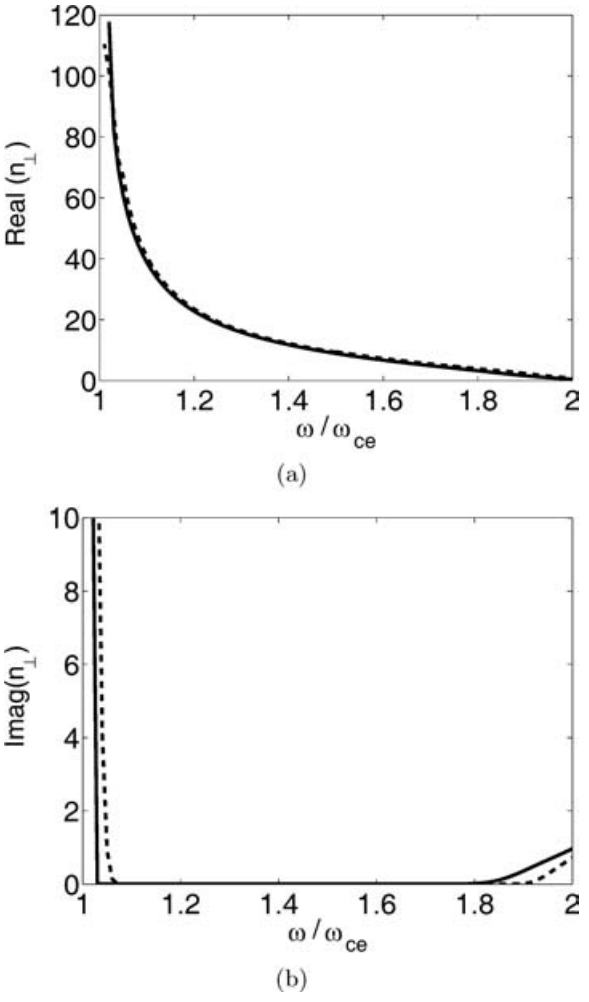


Figure 3. (a) Real and (b) imaginary part of $n_\perp$ versus ω/ω_{ce}. The comparison is between the relativistic (solid) and the non-relativistic (dashed) characteristics of EBWs for $\omega_{pe}/\omega_{ce} = 6$, $n_\parallel = 0.2$, and $T_e = 3$ keV.

5. Kinetic formalism of current drive

As part of the overall scheme to use EBWs for driving plasma currents in a ST, and possibly for achieving steady-state operations, it is important to understand the various physics aspects of EBW current drive. Eventually, one would like to determine the parametric dependence of EBW current drive efficiency on the various plasma parameters, the initial wave spectrum, and the poloidal position from which the waves are launched.

The kinetic model for studying EBW current drive, in its simple form, assumes a toroidally axisymmetric geometry. The magnetic flux surfaces are assumed to be circular and concentric. The steady state, gyro phase averaged kinetic equation is

$$\mathbf{v}_{gc} \cdot \nabla f = C(f) + Q(f), \tag{18}$$

https://doi.org/10.1017/S0022377805003636 Published online by Cambridge University Press

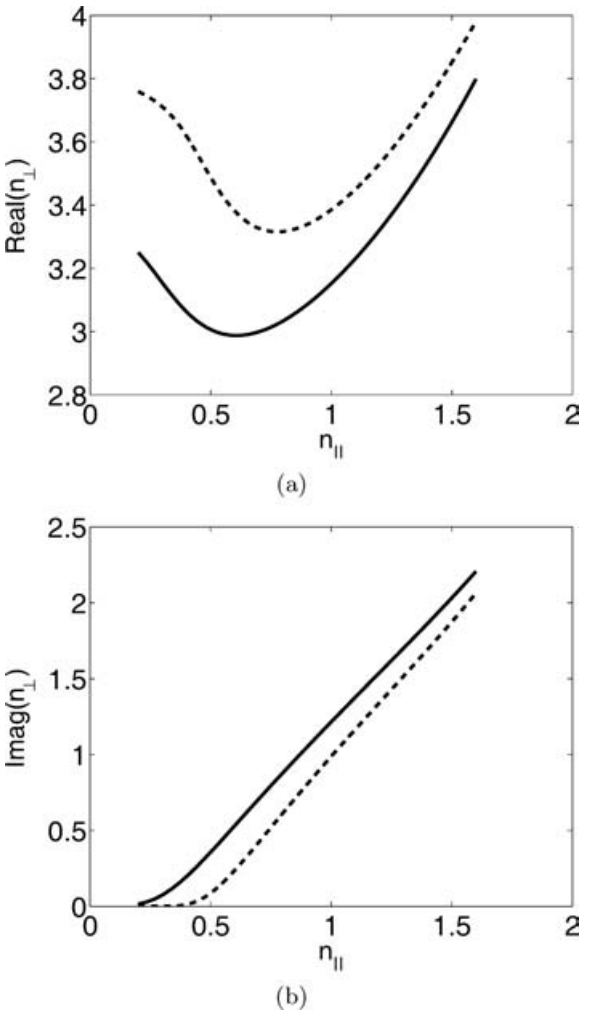


Figure 4. (a) Real and (b) imaginary part of $n_\perp$ versus $n_\parallel$. The comparison is between the relativistic (solid) and the non-relativistic (dashed) characteristics of EBWs for $\omega_{pe}/\omega_{ce} = 6$, $T_e = 3\,\mathrm{keV}$, and $\omega/\omega_{ce} = 1.8$.

where $f = f(r, \theta, p_\perp, p_\parallel)$ is the guiding center electron distribution function which is a function of the radial location r (with respect to the minor axis of the torus) and the poloidal angle θ (measured from the outboard horizontal mid-plane), $\mathbf{v}_{gc}$ is the electron guiding center velocity, C is the collision operator, and Q is the quasilinear diffusion operator due to the interaction of waves with electrons. We can express $\mathbf{v}_{gc}$ as

$$\mathbf{v}_{gc} = v_\parallel \hat{B} + \mathbf{v}_d, \tag{19}$$

where $v_\parallel$ is the electron velocity along the magnetic field line $\hat{B}$ and $\mathbf{v}_d$ is the guiding center drift velocity of the electron. In a ST, as in a tokamak, $v_\parallel \gg v_d$. If we further assume that the characteristic collisional and quasilinear diffusion time scales are much shorter than the drift time scale, then the drift kinetic equation (18) reduces

https://doi.org/10.1017/S0022377805003636 Published online by Cambridge University Press

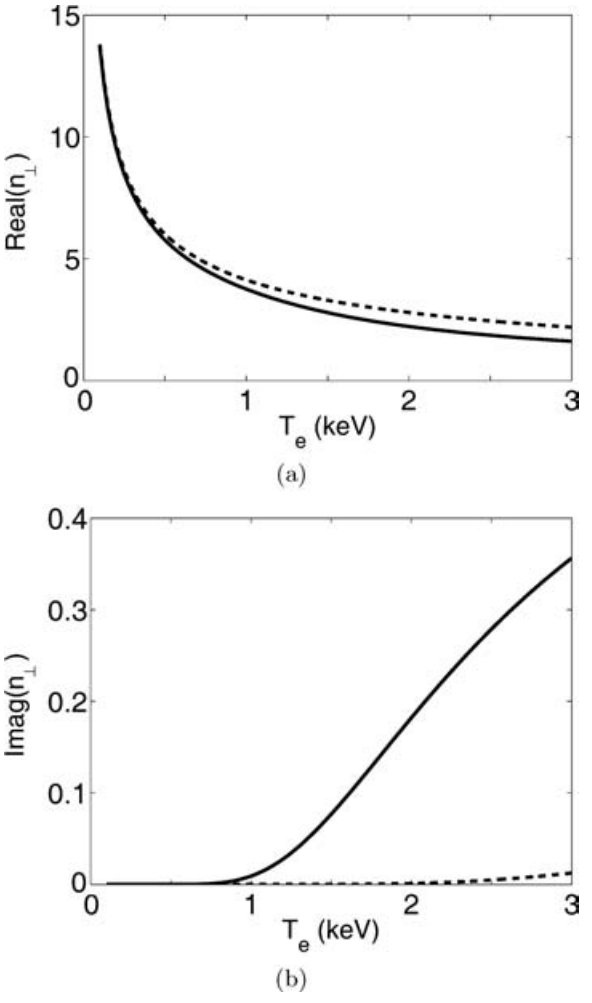


Figure 5. (a) Real and (b) imaginary part of $n_\perp$ versus the electron temperature T_e. The comparison is between the relativistic (solid) and the non-relativistic (dashed) characteristics of EBWs for $\omega_{pe}/\omega_{ce} = 6$, $\omega/\omega_{ce} = 1.9$, and $n_\parallel = 0.2$.

to the Fokker–Planck equation

$$\frac{v_\parallel}{r}\frac{B_\theta}{B}\frac{\partial f}{\partial \theta} = C(f) + Q(f), \tag{20}$$

where B_θ is the poloidal component of the magnetic field. In this equation $f = f(\theta, p_\perp, p_\parallel)$ can be solved for on each flux surface. In the banana approximation where the bounce time of a magnetically trapped electron is much shorter than the collisional detrapping time for such electrons, f is constant along the field lines and symmetric in the trapped region. We define the bounce averaging operator as

$$\{\mathscr{A}\} = \begin{cases} \dfrac{1}{2\pi\tau_b}\dfrac{1}{2}\displaystyle\sum_{\sigma=\pm 1}\int_{-\theta_c}^{\theta_c} d\theta \frac{r}{|v_\parallel|}\frac{B}{B_\theta}\mathscr{A} & \text{for trapped electrons,} \\ \dfrac{1}{2\pi\tau_b}\displaystyle\int_{-\pi}^{\pi} d\theta \frac{r}{|v_\parallel|}\frac{B}{B_\theta}\mathscr{A} & \text{for passing electrons,} \end{cases} \tag{21}$$

https://doi.org/10.1017/S0022377805003636 Published online by Cambridge University Press

where $\sigma = v_\parallel/|v_\parallel|$, and θ_c is the poloidal angle corresponding to the turning point of trapped electrons. The bounce time τ_b is defined for $\mathscr{A} = 1$. Upon bounce averaging (20) we obtain the Fokker–Planck equation

$$\{C(F)\} + \{Q(f)\} = 0. \tag{22}$$

Following Lerche [21], the relativistic quasilinear diffusion operator is

$$Q(f) = \nabla_{\mathbf{p}} \cdot \overline{\overline{D}}^{\mathrm{RF}} \cdot \nabla_{\mathbf{p}} f \tag{23}$$

with the quasilinear diffusion tensor $\overline{\overline{D}}^{\mathrm{RF}}$ given by

$$D_{\perp\perp}^{\mathrm{RF}} = \sum_{n=-\infty}^{\infty} \left(\frac{n\Omega}{\omega}\right) D_n(p_\perp, p_\parallel),$$

$$D_{\perp\parallel}^{\mathrm{RF}} = \sum_{n=-\infty}^{\infty} \frac{p_\perp}{p_\parallel}\frac{n\Omega}{\omega}\left(1 - \frac{n\Omega}{\omega}\right) D_n(p_\perp, p_\parallel),$$

$$D_{\parallel\perp}^{\mathrm{RF}} = D_{\perp\parallel}^{\mathrm{RF}}$$

$$D_{\parallel\parallel}^{\mathrm{RF}} = \sum_{n=-\infty}^{\infty} \frac{p_\perp^2}{p_\parallel^2}\left(1 - \frac{n\Omega}{\omega}\right)^2 D_n(p_\perp, p_\parallel), \tag{24}$$

where, as usual, the subscripts refer to directions relative to the magnetic field, and

$$D_n(p_\perp, p_\parallel) = D_0 \frac{\gamma p_{\mathrm{te}}}{|p_\parallel|}|\Theta_n|^2 \frac{1}{\sqrt{\pi}\Delta n_\parallel} e^{-(n_{\parallel\mathrm{res}} - n_{\parallel 0})^2/\Delta n_\parallel^2} \tag{25}$$

p_{te} is the electron thermal momentum, D_0 is a constant, $\Delta n_\parallel$ is the width in $n_\parallel$ of an EBW beam with a central $n_{\parallel 0}$,

$$\Theta_n = \frac{1}{\sqrt{2}}(E_+ J_{n-1} e^{-i\alpha} + E_- J_{n+1} e^{i\alpha}) + \frac{p_\parallel}{p_\perp} E_\parallel J_n \tag{26}$$

J_n being the nth order Bessel function of the first kind with the argument $(k_\perp v_\perp/\Omega)$, α is the angle between $k_\perp$ and the x direction, E_+ and E_- are the left- and right-hand circularly polarized components of the wave electric field, respectively, and $n_{\parallel\mathrm{res}}$ is the relativistic wave–particle resonance condition

$$n_{\parallel\mathrm{res}} = \frac{mc}{p_\parallel}\left(\gamma - \frac{n\omega_{\mathrm{ce}}}{\omega}\right). \tag{27}$$

A relativistic code DKE [13], which solves the drift kinetic equation including a DC electric field, is being used for studying EBW driven current. DKE includes the relativistic quasilinear diffusion operator discussed above, and the Braams–Karney form of the relativistic (linearized) collision operator [22]. DKE also includes neoclassical effects so that it can be used to kinetically calculate the bootstrap current and its synergy with the wave driven currents [23]. Furthermore, DKE solves the drift kinetic equation for arbitrary flux surface geometries. However, we use a simpler form of DKE, for circular flux surfaces, to solve (22) for the electron distribution function f modified by EBWs. The wave polarizations and the $k_\perp$ needed in (26) are found from the non-relativistic version of R2D2. The effects of relativity on the wave polarization and wavevector will be discussed in a future publication. However, it should be noted that the relativistic form of the quasilinear diffusion operator, which includes the wave–particle resonance condition, is fully retained.

https://doi.org/10.1017/S0022377805003636 Published online by Cambridge University Press

By taking the appropriate moments of f we can solve for the parallel current and the power dissipated and, consequently, evaluate the current drive efficiency $\eta = (J/en_e v_{te})/(P/\nu_e m n_e v_{te}^2)$. Here J is the current density, P is the density of power dissipated, n_e, v_{te}, and ν_e are the local electron density, thermal velocity, and collision frequency, respectively.

6. Current drive by EBWs

In the EC range of frequencies there are two distinct mechanisms for generating plasma currents by the waves. The first mechanism is the Ohkawa effect [14, 15] whereby an asymmetric spectrum (in $n_\parallel$) of the waves diffuses passing electrons into the trapped region. The symmetric collisional de-trapping of the trapped electrons then produces an asymmetry in the electron distribution function. This leads to a current in the plasma in a direction determined by the sign of $k_\parallel$ and whether the approach to the cyclotron resonance is from a direction of increasing or decreasing magnetic field. The second mechanism is the Fisch–Boozer effect [16] whereby an asymmetric wave spectrum leads to an asymmetry in the resistivity of the plasma. This leads to a current in the opposite direction of the phase velocity of the wave spectrum. Both mechanisms rely on the fact that waves in the EC frequency range primarily lead to the perpendicular diffusion of electrons in momentum space. However, the two mechanisms oppose each other. Clearly, to take advantage of the Ohkawa effect the waves need to interact with electrons in the plasma where there is a significant trapped electron population. The Fisch–Boozer effect is more suited to drive currents in the plasma where there is little or no trapped electron population. Our numerical calculations using DKE show that one can take advantage of the two schemes separately in order to efficiently drive currents in different parts of a ST plasma.

The numerical simulations for EBW current drive have been carried out for NSTX-type high-β plasma parameters. We assume that the EBWs are launched along the equatorial plane with a fixed frequency and a fixed initial $n_\parallel$. Along the equatorial plane, $n_\parallel$ does not change significantly as the wave propagates into the plasma [24]. We follow this simpler approach instead of choosing different launch positions of EBWs in order to illustrate the relevant physics of EBW current drive.

The magnetic field is as shown in Fig. 6. In the high-β regime, the poloidal magnetic field is comparable with the toroidal magnetic field in the outer part of the plasma. This creates a dip in the magnetic field profile in the outer middle part of the plasma. The density and temperature profiles are assumed to be of the form

$$n_e = n_E + (n_0 - n_E)\left(1 - \frac{r^2}{a^2}\right)^{1/2},$$
$$T_e = T_E + (T_0 - T_E)\left(1 - \frac{r^2}{a^2}\right)^{2}, \tag{28}$$

where, respectively, $n_0 = 3 \times 10^{19}$ m^{-3} and $T_0 = 3$ keV are the peak electron density and temperature, and $n_E = 0.02\ n_0$ and $T_E = 0.02\ T_0$ are the edge density and temperature. The major radius is taken to be $R_p = 0.9$ m and the plasma radius to be $a = 0.6$ m. We assume that an EBW ray with an input power of 1 MW is launched from the outboard edge of the plasma.

The first series of results illustrates the Ohkawa current drive using EBWs. We chose a wave frequency of 11.8 GHz and $n_\parallel = 1.5$. For this $n_\parallel$ the wave–particle

https://doi.org/10.1017/S0022377805003636 Published online by Cambridge University Press

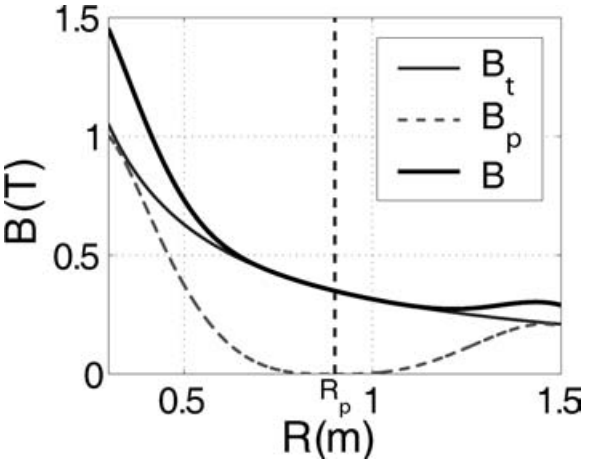


Figure 6. The magnetic field profile along the equatorial plane for a NSTX-type high-β plasma. Here $B_{\rm t}$ and $B_{\rm p}$ are the toroidal and poloidal components of the total magnetic field with magnitude B.

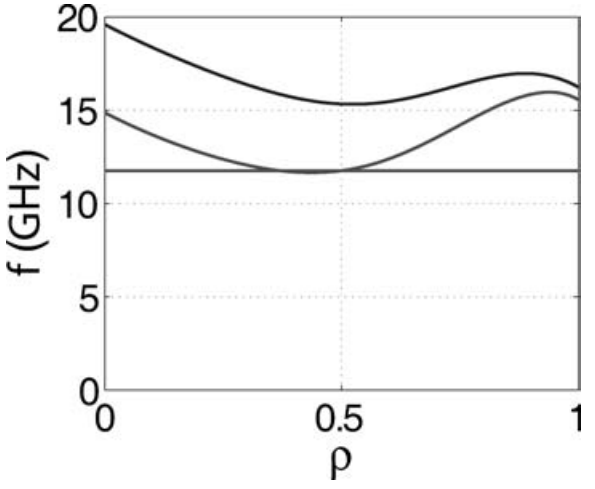


Figure 7. Wave frequency (bottom line), second harmonic of the electron cyclotron frequency $2f_{\rm ce}$ (top curve), and the Doppler-shifted second harmonic electron cyclotron frequency for $n_{\|} = 1.5$ (middle curve) as a function of ρ (radial distance normalized to the minor radius).

resonance surfaces, in electron momentum space, are hyperbolas while the diffusion paths lie along ellipses. Figure 7 shows the Doppler-shifted second harmonic resonance and the wave frequency. The wave frequency is chosen so that the wave is resonant near the bottom of the dip in the magnetic field profile where the field is locally flat. Figure 8(a) shows the current density and the current drive efficiency as a function of ρ, the radial distance normalized to the plasma radius. Figure 8(b) shows the power dissipated along the EBW ray as it propagates into the plasma. The peak current density is about 0.64 MA m^{-2} and the peak power dissipated is about 1.4 MW m^{-3}. At the location of the peak current density the current drive efficiency is $\eta \approx 3.2$. Figures 9(a) and 9(b) illustrate the Ohkawa effect in electron phase

https://doi.org/10.1017/S0022377805003636 Published online by Cambridge University Press

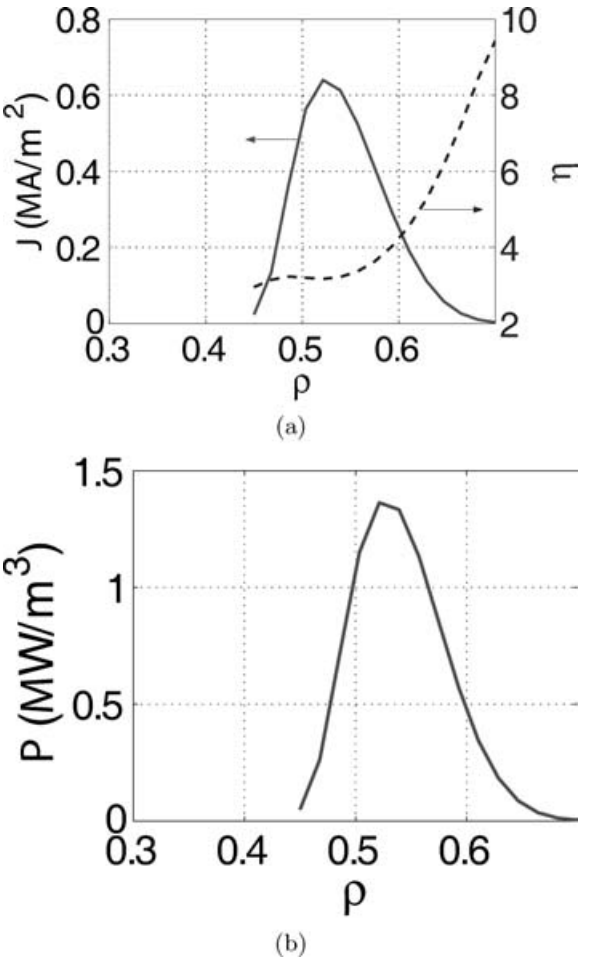


Figure 8. (a) Current density (solid) and efficiency (dashed) as a function of ρ. (b) Power dissipated along the EBW as a function of ρ.

space. Figure 9(a) shows the electron distribution function, in black, as modified by EBWs at the position where the maximum current is generated. The contours in dark grey indicate the magnitude of the EBW diffusion coefficient. The region of maximum diffusion is situated near the trapped/passing boundary leading to a large EBW-induced diffusive trapping of passing electrons. The distribution of the trapped electrons is symmetrized as we have assumed that the mean bounce time of the trapped electrons is the shortest time scale. The collisional scattering of the trapped electrons into the passing region, which occurs over a time scale much longer than the bounce time, is symmetric in phase space across the trapped–passing boundary. This subsequently distorts the distribution function in a region of phase space that is on the opposite side, in $p_\parallel$, from where the EBW wave spectrum exists. Figure 9(b) visually illustrates the modification to the parallel distribution function $F_\parallel$

$$F_\parallel(p_\parallel) = 2\pi \int_0^\infty dp_\perp \, p_\perp f(p_\perp, p_\parallel) \tag{29}$$

https://doi.org/10.1017/S0022377805003636 Published online by Cambridge University Press

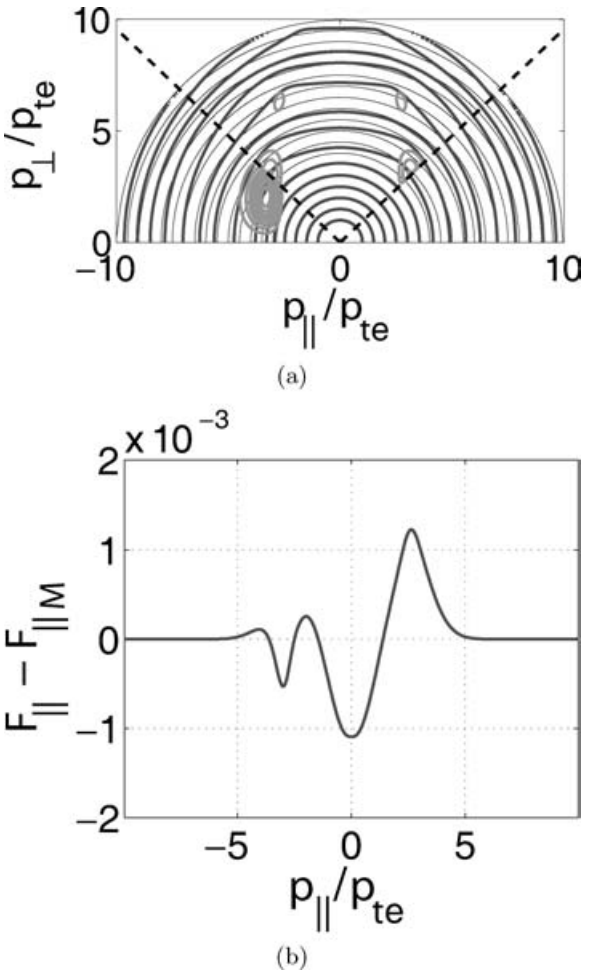


Figure 9. (a) Contours of the Maxwellian distribution (light grey) and the distribution function in the presence of EBW diffusion coefficient (black). The contours in dark grey give the magnitude of the EBW diffusion coefficient. The dashed black lines indicate the trapped–passing boundary. These contours are obtained at the spatial location where the EBW driven current density in Fig. 8(a) is a maximum. (b) The parallel component of the RF driven distribution function, with the Maxwellian contribution subtracted out, as a function $p_\parallel$ normalized to the thermal momentum $p_{\rm te}$.

in the presence of EBWs after the corresponding Maxwellian part $F_{\parallel \rm M}$ has been subtracted out. We note that a modification to $F_\parallel - F_{\parallel \rm M}$ occurs for positive $p_\parallel$ when the EBW induced diffusion, in the passing region, is for negative $p_\parallel$. The scattering into the trapped region by EBWs and the subsequent collisional detrapping connect the two regions in $p_\parallel$ space.

The second series of results illustrate the Fisch–Boozer current drive using EBWs. In this set the wave frequency is chosen to be 19.5 GHz and $n_\parallel = 0.5$. For this $n_\parallel$ the wave–particle resonance surfaces are ellipses while the diffusion paths lie along hyperbolas. Figure 10 shows that for these parameters the Doppler-shifted third harmonic of the EC frequency, in the outer half of the plasma, can be avoided by

https://doi.org/10.1017/S0022377805003636 Published online by Cambridge University Press

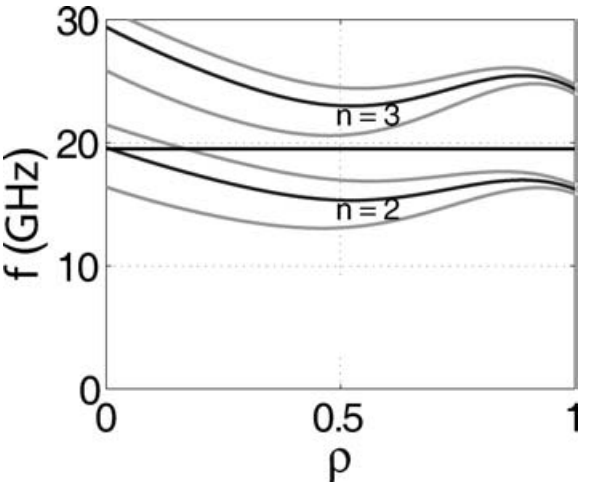


Figure 10. Wave frequency f (black straight line), second $n = 2$ and third $n = 3$ harmonics of the EC frequency (black curved lines), and the Doppler-shifted resonances (grey) for $n_\parallel = 0.5$ as a function of ρ. The two green curves around each blue curve are due to the positive and negative signs in the Doppler shifts.

the EBW. The wave frequency matches the Doppler-shifted second harmonic of the EC frequency near the core of the plasma. Figure 11(a) shows the current density and the current drive efficiency as a function of ρ and Fig. 11(b) shows the power dissipated. For this case, the peak current density is about 2.6 MA m^{-2} and the peak dissipated power density is about 6.1 MW m^{-3}. At the location of the peak current density the current drive efficiency is $\eta \approx 1.9$. The Fisch–Boozer effect in phase space is shown in Figs 12(a) and 12(b). The EBW diffusion coefficient is maximized further away from the trapped–passing boundary than in Fig. 9(a) for the Ohkawa case. This leads to an asymmetric change, in $p_\parallel$, in the plasma resistivity which, in turn, generates current in the plasma. The parallel wave spectrum for the Fisch–Boozer scheme is in the opposite direction to that for the Ohkawa scheme when both schemes are used to generate plasma current at the same location and in the same direction. Figures 12(a) and 12(b) also show that some of the electrons affected by the EBW are scattered in the negative $p_\parallel$ direction. This occurs through the wave-induced diffusion of the electrons into the trapped region and collisional de-trapping out of the region. Consequently, there is a decrease in the current generated by electrons with positive $p_\parallel$. This result is similar to the Ohkawa case shown in Fig. 9(b) where the electrons with negative $p_\parallel$ decrease the current generated by the electrons scattered in the positive $p_\parallel$ direction.

The current drive efficiencies of both the Fisch–Boozer and Ohkawa mechanisms discussed above are significantly better than those obtained for conventional EC current drive. This is primarily because EBWs are damped by more energetic electrons. They are also strongly absorbed at the Doppler-shifted resonances of higher harmonics of the EC frequency.

7. Conclusions

Our calculations show that relativistic effects are important in describing the propagation and damping of EBWs in ST plasmas. A consequence of the relativistic

https://doi.org/10.1017/S0022377805003636 Published online by Cambridge University Press

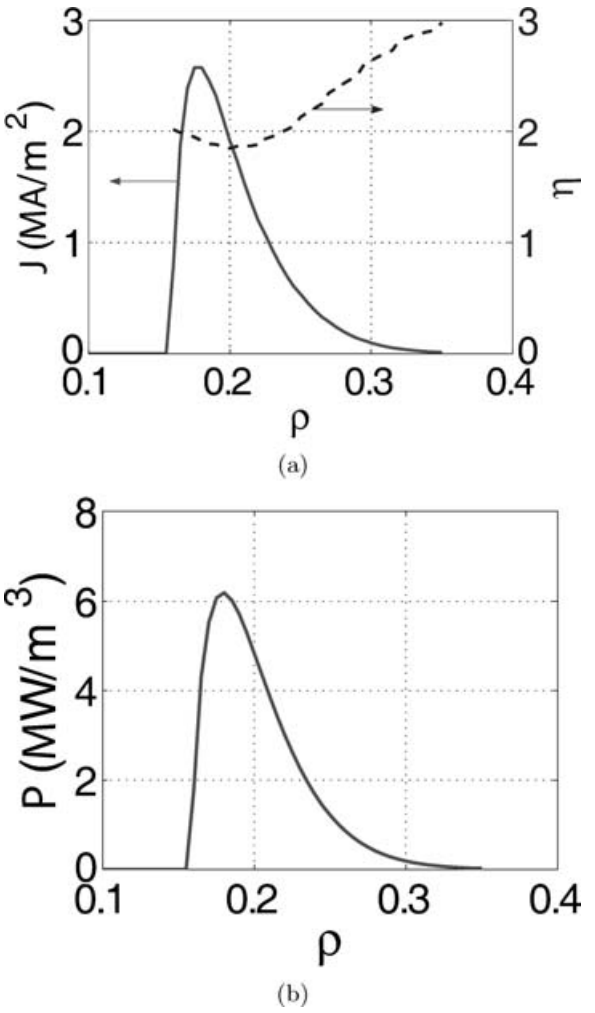


Figure 11. (a) Current density (solid) and efficiency (dashed) as a function of ρ. (b) Power dissipated along the EBW as a function of ρ.

effects is that EBWs could propagate and damp in regions of the plasma which are very different from those one would get by considering just the non-relativistic dispersion relation. From an experimental point of view this is a significant consequence. For example, if EBW current drive is needed to control the current profile so as to curb the growth of instabilities, such as the neoclassical tearing mode, the choice of EBW wave parameters and launch position would be guided by the location of where the waves need to interact with electrons. We are now in the process of developing a fully relativistic ray-tracing code to study the propagation of EBWs in a toroidal geometry.

EBWs offer different possibilities for generating plasma currents. In the outer half of a ST plasma, where there is a significant fraction of trapped electrons, the EBWs could be used to drive currents through the Ohkawa scheme. In the core of the plasma, where the trapped electron fraction is smaller, the conventional

https://doi.org/10.1017/S0022377805003636 Published online by Cambridge University Press

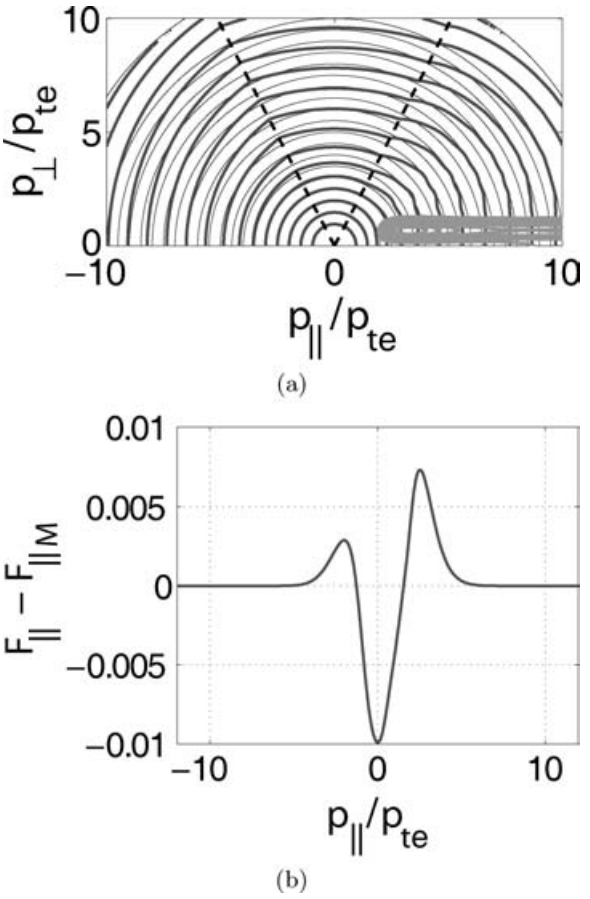


Figure 12. (a) Contours of the Maxwellian distribution (light grey) and the distribution function in the presence of EBW diffusion coefficient (black). The contours in dark grey give the magnitude of the EBW diffusion coefficient. The dashed black lines indicate the trapped–passing boundary. These contours are obtained at the spatial location where the EBW driven current density in Fig. 11(a) is a maximum. (b) The parallel component of the radiofrequency driven distribution function, with the Maxwellian contribution subtracted out, as a function $p_\parallel/p_{\rm te}$.

Fisch–Boozer scheme would be more suitable for inducing plasma currents. Thus, the EBW spectrum and the launch position of the waves could be tailored according to the desired needs for current generation and current profile control. In the EC frequency range the EBWs tend to interact with more energetic electrons than the conventional X and O modes. Also, EBWs are effectively absorbed by these energetic and less collisional electrons in the vicinity of the Doppler-shifted EC resonances. Consequently, the EBW current drive efficiency can be significantly higher than that for conventional EC current drive.

Detailed studies on relativistic effects in EBW propagation and damping, and on the EBW driven current are continuing. Along with the previous results on coupling and excitation of EBWs, the results from these studies will provide a general basis for defining the role of EBWs in present-day experiments and future ST power plants.

https://doi.org/10.1017/S0022377805003636 Published online by Cambridge University Press

Acknowledgements

The authors are grateful to Professor Padma Kant Shukla and Dr Robert Bingham for encouraging us to write this paper. This work was supported by DOE Grant Numbers DE-FG02-91ER-54109 and DE-FG02-99ER-54521.

References

[1] One, M., et al. 1998 *Proceedings of the 17th International Conference on Fusion Energy 1998 (Yokohama, 1998)*. Vienna: IAEA (CD-ROM file ICP/01). http://www.iaea.org/programmes/ripe/physics/fec1998/pdf/icp_01.pdf.

[2] Sykes, A. 1998 *Proceedings of the 17th International Conference on Fusion Energy 1998 (Yokohama, 1998)*. Vienna: IAEA (CD-ROM file OV2/5). http://www.iaea.org/programmes/ripe/physics/fec1998/pdf/ov2_5.pdf.

[3] Ram, A. K. and Schultz, S. D. 2000 *Phys. Plasmas* **7**, 4084.

[4] Preinhaelter, J. and Kopecky, V. 1973 *J. Plasma Phys.* **10**, 1.

[5] Ram, A. K. and Bers, A. 2003 *Nucl. Fusion* **43**, 1305.

[6] Ram, A. K., Bers, A. and Lashmore-Davies, C. N. 2002 *Phys. Plasmas* **9**, 409.

[7] Laqua, H. P. 2003 *Proceedings of the 15th Topical Conference on RF Power in Plasmas (AIP Conference Proceedings, 694)* (ed. C. B. Forest). Melville, NY: AIP, p. 15.

[8] Cairns, R. A., Owen, J. and Lashmore-Davies, C. N. 1983 *Phys. Fluids* **26**, 3475.

[9] Bornatici, M., Cano, R., De Barbieri, O. and Engelmann, F. 1983 *Nucl. Fusion* **23**, 1153.

[10] LeClair, G., Shkarofsky, I. P., Demers, Y. and Mercier, J.-F. 1997 *Proceedings of the 12th Topical Conference on RF Power in Plasmas (AIP Conference Proceedings, 403)* (ed. P. M. Ryan and T. Intrator). New York: Woodbury, p. 219.

[11] Forest, C. B., Chattopadhyay, P. K., Harvey, R. W. and Smirnov, A. P. 2000 *Phys. Plasmas* **7**, 1352.

[12] Taylor, G., et al. 2004 *Phys. Plasmas* **11**, 4733.

[13] Peysson, Y., Decker, J. and Harvey, R. W. 2003 *Proceedings of the 15th Topical Conference on RF Power in Plasmas (AIP Conference Proceedings, 694)* (ed. C. B. Forest). Melville, NY: AIP, p. 495.

[14] Ohkawa, T. 1976 *Report No. GA-A13847*, General Atomics.

[15] More recently Ohkawa current drive using waves in the electron cyclotron range of frequencies has been discussed by: Decker, J. 2003 *Proceedings of the 15th Topical Conference on RF Power in Plasmas (AIP Conference Proceedings, 694)* (ed. C. B. Forest). Melville, NY: AIP, p. 447.

[16] Fisch, N. J. and Boozer, A. 1980 *Phys. Rev. Lett.* **45**, 720.

[17] Trubnikov, B. A. 1959 *Plasma Physics and the Problem of Controlled Thermonuclear Reaction*, Vol. III (ed. Leontovich, M. A.). New York: Pergamon.

[18] Shkarofsky, I. P. 1966 *Phys. Fluids* **9**, 561.
Shkarofsky, I. P. 1966 *Phys. Fluids* **9**, 570.

[19] Stix, T. H. 1992 *Theory of Plasma Waves*, 2nd edn. New York: Wiley.

[20] Weiss, I. 1985 *J. Comput. Phys.* **61**, 403.

[21] Lerche, I. 1968 *Phys. Fluids* **11**, 720.

[22] Braams, B. J. and Karney, C. F. F. 1989 *Phys. Fluids* B **1**, 1355.

[23] Decker, J., Peysson, Y., Bers, A. and Ram, A. K. 2002 *Proceedings of the EC-12 Conference*, Aix-en-Provence, France.
Decker, J., Peysson, Y., Bers, A. and Ram, A. K. 2002 *29th EPS Conference on Plasma Physics and Controlled Fusion*, Montreux, Switzerland.
Schultz, S. D., Bers, A. and Ram, A. K. 1999 *AIP Conference Proceedings*, **485**, 317
Schultz, S. D. 1999 *PhD Thesis*, Department of Physics, MIT.

[24] Ram, A. K. and Bers, A. 1991 *Phys. Fluids* B **3**, 1059.

https://doi.org/10.1017/S0022377805003636 Published online by Cambridge University Press